JACS
JOURNAL OF THE AMERICAN CHEMICAL SOCIETY
Communication
Cite This: J. Am. Chem. Soc. 2019, 141, 7670−7674
pubs.acs.org/JACS

Copper-Containing Carbon Feedstock for Growing Superclean Graphene

Kaicheng Jia,[†,¶] Jincan Zhang,[†,‡,¶] Li Lin,[†,¶] Zhenzhu Li,[§] Jing Gao,[§] Luzhao Sun,[†,‡] Ruiwen Xue,[∥] Jiayu Li,[⊥] Ning Kang,[⊥] Zhengtang Luo,[∥] Mark H. Rummeli,[§] Hailin Peng,*[,†,#] and Zhongfan Liu*[,†,#]

[†]Center for Nanochemistry, Beijing Science and Engineering Center for Nanocarbons, Beijing National Laboratory for Molecular Sciences, College of Chemistry and Molecular Engineering, Peking University, Beijing 100871, People's Republic of China

[‡]Academy for Advanced Interdisciplinary Studies, Peking University, Beijing 100871, People's Republic of China

[§]Soochow Institute for Energy and Materials InnovationS, Soochow University, Suzhou 215006, People's Republic of China

[⊥]Beijing Key Laboratory of Quantum Devices, Key Laboratory for the Physics and Chemistry of Nanodevices, and Department of Electronics, Peking University, Beijing 100871, People's Republic of China

[∥]Department of Chemical and Biological Engineering, Hong Kong University of Science and Technology, Clear Water Bay, Hong Kong SAR 999077, People's Republic of China

[#]Beijing Graphene Institute (BGI), Beijing 100095, People's Republic of China

Supporting Information

ABSTRACT: Chemical vapor deposition (CVD) enables the large-scale growth of high-quality graphene film and exhibits considerable potential for the industrial production of graphene. However, CVD-grown graphene film contains surface contamination, which in turn hinders its potential applications, for example, in electrical and optoelectronic devices and in graphene-membrane-based applications. To solve this issue, we demonstrated a modified gas-phase reaction to achieve the large-scale growth of contamination-free graphene film, i.e., superclean graphene, using a metal-containing molecule, copper(II) acetate, $Cu(OAc)_2$, as the carbon source. During high-temperature CVD, the Cu-containing carbon source significantly increased the Cu content in the gas phase, which in turn suppressed the formation of contamination on the graphene surface by ensuring sufficient decomposition of the carbon feedstock. The as-received graphene with a surface cleanness of about 99% showed enhanced optical and electrical properties. This study opens a new avenue for improving graphene quality with respect to surface cleanness and provides new insight into the mechanism of graphene growth through the gas-phase reaction pathway.

Chemical vapor deposition (CVD) has shown great promise for the scalable production of carbon nanomaterials with promising controllability, uniformity, and quality.[1−4] However, surface contamination is sometimes inevitable in the high-temperature CVD process and degrades the growth behavior and properties of the received materials.[5] Given the two-dimensional nature of CVD-grown graphene, surface contamination of graphene highly degrades its intrinsic properties[6] and impedes its applications in many fields, such as electrical and optoelectronic devices, e.g., organic light-emitting diodes.[7] Therefore, the preparation of contamination-free graphene is essential for its future industrial applications.[8]

To date, post-treatment processing techniques, including high-temperature annealing[9] and plasma-assisted etching,[10] have been proposed to remove surface contamination on graphene, mainly by removing the transfer-related polymer residues and airborne contamination.[11] However, the reported cleanness of graphene after these routines is still far from ideal,[9,10] which indicates that the dominant factors for improving cleanness are still unclear. The lack of consensus over the origin of surface contamination has inspired us to consider the contribution of high-temperature CVD to the formation of surface contamination on graphene.

Herein, the main contamination on the CVD graphene surface is found to be amorphous carbon, which is introduced during the high-temperature CVD growth, rather than the transfer step. Such an amorphous structure has been previously regarded as a byproduct during the CVD growth of carbon nanotubes.[12] Based on the understanding of the formation mechanism of amorphous carbon on graphene during high-temperature CVD,[13] we developed an efficient method to directly grow superclean graphene with an areal cleanness of ∼99% using $Cu(OAc)_2$ as a new carbon feedstock (Figures S1 and S2). The improved cleanness was mainly attributed to the continuous supply of Cu in the gas phase during graphene growth, which ensured sufficient decomposition of the carbon species by reducing its activation energy. The improved cleanness of grown graphene further ensured a reduced amount of polymer residues on graphene in the subsequent transfer step onto functional substrates. The superclean surface of graphene contributed to its improved optical and electrical properties, thus providing new opportunities for future graphene-based applications.

Received: February 22, 2019
Published: May 6, 2019

DOI: 10.1021/jacs.9b02068
J. Am. Chem. Soc. 2019, 141, 7670−7674

In a conventional CVD system for high-quality graphene growth, the decomposition degree of the carbon feedstocks, for example, dehydrogenation of CH_4 to CH_3, CH_2, and CH,[14] is highly dependent on the metal catalyst content,[15] especially for gas-phase reactions, and active carbon species accumulated in the boundary layer have a significant impact on the growth behavior of graphene.[16] However, the ability of Cu vapor to decompose CH_4 during graphene growth is limited considering that the saturated vapor pressure of Cu is less than 3×10^{-7} bar (~1000 °C)[17] and Cu vapor content gradually decreased with the increasing coverage of graphene on the Cu surface, according to the surface-mediated growth mechanism.[18] Therefore, when using a typical carbon source such as CH_4, the insufficient supply of Cu vapor during graphene growth is a common problem, which would lead to a lower decomposition degree of the carbon source in the gas phase, thus leading to the formation of amorphous carbon (Figure 1a, top). The presence of amorphous carbon on the CVD-grown graphene surface was verified using atomic force microscopy (AFM), with an average thickness of 2.4 nm (Figure 1b). Meanwhile, the universal distribution of amorphous carbon on the graphene surface was confirmed by a transmission electron microscopy (TEM) image, where amorphous carbon showed a darker contrast and induced an obvious diffraction ring in the corresponding fast Fourier transform (FFT) (Figure 1c, inset). Clearly, the areas of the continuous clean regions were only tens of nanometers, and the area ratio of the clean regions was less than 50%, consistent with previously reported values (Figure S3).[9,19]

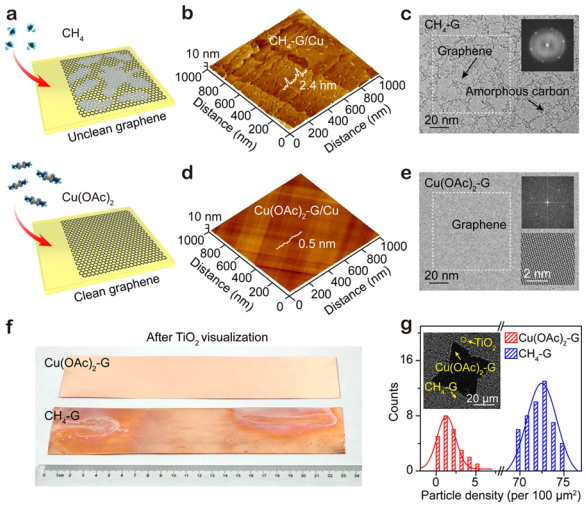

Figure 1. Cleanness improvement of $Cu(OAc)_2$-derived graphene. (a) Cleanness comparison between $Cu(OAc)_2$- and CH_4-derived graphene. Top: Schematic of formation of amorphous carbon on the graphene surface using CH_4 as the carbon source. Bottom: Schematic of growth of superclean graphene using $Cu(OAc)_2$ as the carbon source. (b, c) AFM (b) and TEM (c) images of unclean graphene with observable presence of amorphous carbon obtained using CH_4 as the carbon source. Inset of (c): FFT pattern of the square region in (c). (d, e) AFM (d) and TEM (e) images of clean graphene obtained using $Cu(OAc)_2$ as the carbon source. Insets in (e): FFT pattern of the corresponding TEM image (top) and HRTEM image of graphene film with lattice resolution (bottom). (f) Photograph of large-area graphene films grown by $Cu(OAc)_2$ (top) and CH_4 (bottom) after TiO_2 visualization using $TiCl_4$ evaporation. (g) Density of TiO_2 nanoparticles on clean (red) and unclean (blue) graphene. Inset: SEM image of graphene grown using $Cu(OAc)_2$ and CH_4 sequentially, with clear distributional difference of TiO_2 nanoparticles.

Based on the understanding of the gas-phase reaction mechanism, we found that the Cu-containing carbon source, $Cu(OAc)_2$, could continuously supply Cu to the boundary layer during graphene growth. This guaranteed the sufficient decomposition of the carbon species, thus suppressing the formation of amorphous carbon. In this regard, a higher degree of cleanness (~99%) was achieved. The elimination of surface contamination on graphene was confirmed by the AFM (surface roughness <0.5 nm) (Figure 1d) and TEM characterization (Figure 1e), where no obvious amorphous carbon was observed. The clearly visible perfect hexagonal graphene lattice in the high-resolution TEM (HRTEM) image (Figure 1e) and noise-level D-band intensity in Raman spectra of the graphene grown from $Cu(OAc)_2$ (Figure S4) both indicated the potential of $Cu(OAc)_2$ in the growth of defect-free graphene with enhanced surface cleanness.

Evaluation of graphene cleanness on a large scale can be achieved using the selective deposition behavior of TiO_2 particles formed from $TiCl_4$ vapor (Figure S5).[20] Owing to the presence of abundant dangling bonds, the amorphous carbon on an unclean graphene surface would adsorb a large number of TiO_2 particles and become multicolored upon contacting $TiCl_4$ vapor. In contrast, clean graphene film would retain its original color after TiO_2 deposition (Figure 1f and Figure S6). To further confirm the contribution of $Cu(OAc)_2$ to cleanness enhancement and exclude the influence of other factors, we used $Cu(OAc)_2$ as the carbon feedstock to initiate the nucleation of graphene and then changed it to ^{13}C-labeled CH_4 for further epitaxial growth. Thus, a structure with $Cu(OAc)_2$-grown nuclei and a CH_4-grown shell was formed, as confirmed by the carbon isotope distribution verified by Raman mapping (Figure S7). After TiO_2 visualization, the average density of the TiO_2 nanoparticles in the $Cu(OAc)_2$-derived region (about 2 nanoparticles per 100 μm^2) was clearly lower than that in the CH_4-derived region (about 73 nanoparticles per 100 μm^2) (Figure 1g), further verifying the improved cleanness of graphene grown by $Cu(OAc)_2$.

For a more detailed understanding of the role of Cu vapor in the cleanness enhancement of graphene, density functional theory calculations of the dehydrogenation process of carbon species were performed. CH_4 underwent four steps to achieve complete decomposition, and the energy barriers significantly decreased with the participation of Cu catalyst (Figure 2a). For example, the threshold barrier for CH_4 decomposed into CH_3 was up to 1.29 eV, whereas with the Cu catalyst, this value sharply decreased to −0.04 eV. Thus, according to the Arrhenius equation, the reaction rate of thermal decomposition was much lower than that of catalytic decomposition in the gas phase, even though both processes occurred in the high-temperature CVD system. On this basis, the partial pressure of Cu vapor became the vital factor deciding the dehydrogenation degree of carbon species. Therefore, sufficient Cu catalyst supplied by $Cu(OAc)_2$ (Figures S8−10) could promote the decomposition of the carbon species in the gas phase to generate highly dehydrogenated CH_x active species and further decrease the formation probability of amorphous carbon contamination (Figure 2b). In contrast, a large quantity of carbon species, e.g., CH_3, would accumulate in the boundary layer and generate amorphous carbon contamination on the graphene surface when CH_4 was used,[21] owing to the limited amount of Cu vapor contributed by Cu foil.

DOI: 10.1021/jacs.9b02068
J. Am. Chem. Soc. 2019, 141, 7670−7674

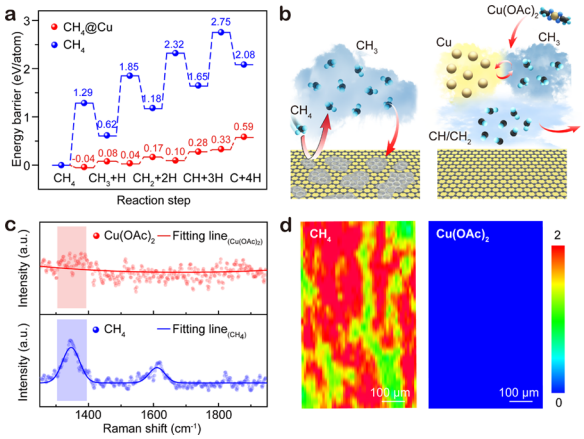

Figure 2. Theoretical investigation of the contribution of $Cu(OAc)_2$ to the cleanness improvement. (a) Calculated energy barriers of CH_4 dehydrogenation in the gas phase with (red) and without (blue) Cu catalyst (vapor). (b) Schematics of the role of Cu vapor in the gas phase in promoting the decomposition of the carbon species and suppressing the formation of amorphous carbon. (c, d) Typical Raman spectra (c) of the species collected in the boundary layer during graphene growth using $Cu(OAc)_2$ (red) and CH_4 (blue) and corresponding D-peak mapping (d).

Meanwhile, the species on Al_2O_3 molecular sieves collected from the boundary layer during graphene growth was characterized using a Raman spectrometer (Figure S9). When CH_4 was used, a prominent D-band signal was detected, confirming formation of abundant carbon species with poor crystallinity, i.e., amorphous carbon (Figure 2c and d). In contrast, no signals of amorphous carbon were detected when using $Cu(OAc)_2$, revealing its advantages to efficiently suppressing formation of contamination. Besides, no improvement of graphene cleanness was observed when using acetic acid as carbon feedstock or adding CO_2 through the synthesis of graphene (Figure S11), further confirming the importance of additional Cu supply.

Generally, a polymer-assisted transfer method is required for further applications of graphene,[22] whereas graphene film synthesized using conventional CH_4-based CVD was usually covered by a high density of polymer residues (Figure S12).[7] Notably, clean graphene grown using $Cu(OAc)_2$ showed a clear decrease in the amount of transfer-induced PMMA residues, with no additional polymer particles observed in the AFM image (Figure 3a) and roughness comparable to that of mechanically exfoliated monolayer graphene (Figure 3b). In addition, time-of-flight secondary ion mass spectrometry was conducted to clarify the reduced transfer-related contamination on a clean graphene surface using deuterated PMMA (^{2}H-PMMA).[23] After removing ^{2}H-PMMA using acetone, a prominent polymer-related ^{2}H peak was observed only in the spectrum of unclean graphene (Figure S13), further confirming the advantages of $Cu(OAc)_2$. The presence of polymer residues could alter the frictional features of the graphene surface.[24] That is, $Cu(OAc)_2$-derived clean graphene exhibited a lower friction similar to that of exfoliated graphene, much lower than that of CH_4-derived unclean graphene and pure PMMA film (Figure 3c,d and Figure S14).

Clean graphene film exhibited improved optical and electrical properties, probably owing to the less photon absorption and electron scattering. The clean graphene grown by $Cu(OAc)_2$ exhibited a lighter contrast after transfer to quartz substrates

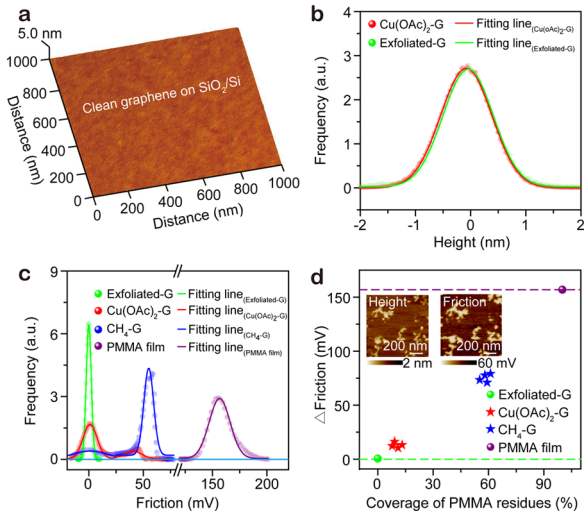

Figure 3. Surface cleanness of transferred graphene films. (a) AFM image of clean graphene film transferred onto a SiO_2/Si substrate with the assistance of poly(methyl methacrylate) (PMMA). (b) Height histograms of clean graphene film (red) in (a) and exfoliated graphene (green). (c) Friction histograms of transferred graphene film grown by $Cu(OAc)_2$ (red) and CH_4 (blue), with exfoliated graphene (green) and PMMA film (purple) as references. (d) Friction comparison of the four samples listed in (c). Inset: In situ height and friction images of unclean graphene on a SiO_2/Si substrate.

than its unclean counterpart (Figure 4a and Figure S15), with its light transmittance close to the theoretical simulation results.[25] Multilayer clean graphene grown by $Cu(OAc)_2$ fabricated via layer-by-layer transfer also had high transmittance (Figure 4b). Field effect transistor mobility of graphene grown by $Cu(OAc)_2$ was about 9700 $cm^2/(Vs)$ at room temperature on a SiO_2/Si substrate (Figure S16). Meanwhile, based on the fabrication of

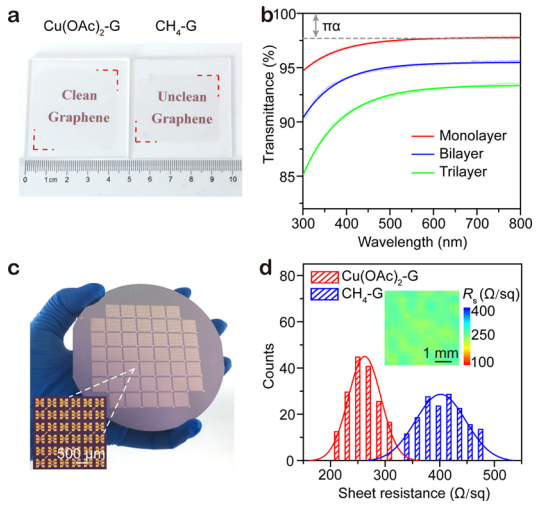

Figure 4. Optical and electrical properties of clean graphene grown by $Cu(OAc)_2$. (a) Photograph of large-area clean (left) and unclean (right) graphene film transferred onto quartz substrates obtained using $Cu(OAc)_2$ and CH_4 as carbon feedstocks, respectively. (b) UV−vis spectra of monolayer, bilayer, and trilayer graphene films grown by $Cu(OAc)_2$ transferred onto quartz substrates. (c) Photograph of graphene device patterns on a 4 in. SiO_2/Si wafer. Inset: Optical microscopy image of graphene devices. (d) Statistical results of sheet resistance of graphene grown by $Cu(OAc)_2$ (red) and CH_4 (blue). Inset: Sheet resistance mapping of clean graphene film.

DOI: 10.1021/jacs.9b02068
J. Am. Chem. Soc. 2019, 141, 7670−7674

patterns of Hall-bar devices on a 4 in. SiO_2/Si wafer (Figure 4c), $Cu(OAc)_2$-derived graphene film also exhibited a narrow distribution of sheet resistance with an average value of ∼270 Ω/sq (Figure 4d and Figure S17).

In conclusion, we demonstrated a novel carbon feedstock to grow high-quality graphene with significantly improved surface cleanness. The as-prepared superclean graphene, with >99% surface clean region, exhibited clearly reduced polymer residue amounts on its surface after transfer and improved optical and electrical properties. This study provides new insights into gas-phase reaction engineering to obtain high-quality superclean graphene films and paves the way for the large-scale production of graphene films with improved properties for future applications.

■ ASSOCIATED CONTENT

Supporting Information

The Supporting Information is available free of charge on the ACS Publications website at DOI: 10.1021/jacs.9b02068.

Experimental details, supplementary figures (PDF)

■ AUTHOR INFORMATION

Corresponding Authors

*hlpeng@pku.edu.cn
*zfliu@pku.edu.cn

ORCID

Ning Kang: 0000-0003-4478-8402
Zhengtang Luo: 0000-0002-5134-9240
Hailin Peng: 0000-0003-1569-0238
Zhongfan Liu: 0000-0003-0065-7988

Author Contributions

¶K. Jia, J. Zhang, and L. Lin contributed equally to this work.

Notes

The authors declare no competing financial interest.

■ ACKNOWLEDGMENTS

This work was financially supported by the Beijing Municipal Science & Technology Commission (No. Z181100004818001), the National Basic Research Program of China (Nos. 2014CB932500 and 2016YFA0200101), and the National Natural Science Foundation of China (Nos. 21525310, 51432002, and 51520105003). We also acknowledge Beijing National Laboratory for Molecular Science for the support. We thank Lutao Weng at the Hong Kong University of Science and Technology for help with ToF-SIMS characterization.

■ REFERENCES

(1) Li, X. S.; Cai, W. W.; An, J. H.; Kim, S.; Nah, J.; Yang, D. X.; Piner, R.; Velamakanni, A.; Jung, I.; Tutuc, E.; Banerjee, S. K.; Colombo, L.; Ruoff, R. S. Large-Area Synthesis of High-Quality and Uniform Graphene Films on Copper Foils. *Science* **2009**, *324*, 1312−1314.

(2) Bae, S.; Kim, H.; Lee, Y.; Xu, X.; Park, J.-S.; Zheng, Y.; Balakrishnan, J.; Lei, T.; Kim, H. R.; Song, Y. I. Roll-to-Roll Production of 30-in. Graphene Films for Transparent Electrodes. *Nat. Nanotechnol.* **2010**, *5*, 574.

(3) Hao, Y.; Bharathi, M.; Wang, L.; Liu, Y.; Chen, H.; Nie, S.; Wang, X.; Chou, H.; Tan, C.; Fallahazad, B. The Role of Surface Oxygen in the Growth of Large Single-Crystal Graphene on Copper. *Science* **2013**, *342*, 1243879.

(4) Zeng, M.; Wang, L.; Liu, J.; Zhang, T.; Xue, H.; Xiao, Y.; Qin, Z.; Fu, L. Self-Assembly of Graphene Single Crystals with Uniform Size and Orientation: The First 2D Super-Ordered Structure. *J. Am. Chem. Soc.* **2016**, *138*, 7812−7815.

(5) Hata, K.; Futaba, D. N.; Mizuno, K.; Namai, T.; Yumura, M.; Iijima, S. Water-Assisted Highly Efficient Synthesis of Impurity- Free Single-Walled Carbon Nanotubes. *Science* **2004**, *306*, 1362−1364.

(6) Chen, J.-H.; Jang, C.; Xiao, S.; Ishigami, M.; Fuhrer, M. S. Intrinsic and Extrinsic Performance Limits of Graphene Devices on SiO_2. *Nat. Nanotechnol.* **2008**, *3*, 206.

(7) Zhang, Z.; Du, J.; Zhang, D.; Sun, H.; Yin, L.; Ma, L.; Chen, J.; Ma, D.; Cheng, H.-M.; Ren, W. Rosin-Enabled Ultraclean and Damage-free Transfer of Graphene for Large-Area Flexible Organic Light-Emitting Diodes. *Nat. Commun.* **2017**, *8*, 14560.

(8) Novoselov, K. S.; Fal, V.; Colombo, L.; Gellert, P.; Schwab, M.; Kim, K. A Roadmap for Graphene. *Nature* **2012**, *490*, 192.

(9) Lin, Y.-C.; Lu, C.-C.; Yeh, C.-H.; Jin, C.; Suenaga, K.; Chiu, P.-W. Graphene Annealing: How Clean Can It Be? *Nano Lett.* **2012**, *12*, 414−419.

(10) Cunge, G.; Ferrah, D.; Petit-Etienne, C.; Davydova, A.; Okuno, H.; Kalita, D.; Bouchiat, V.; Renault, O. Dry Efficient Cleaning of Poly-Methyl-Methacrylate Residues from Graphene with High-Density H_2 and H_2-N_2 Plasmas. *J. Appl. Phys.* **2015**, *118*, 123302.

(11) Li, Z.; Wang, Y.; Kozbial, A.; Shenoy, G.; Zhou, F.; McGinley, R.; Ireland, P.; Morganstein, B.; Kunkel, A.; Surwade, S. P. Effect of Airborne Contaminants on the Wettability of Supported Graphene and Graphite. *Nat. Mater.* **2013**, *12*, 925.

(12) Schuenemann, C.; Schaeffel, F.; Bachmatiuk, A.; Queitsch, U.; Sparing, M.; Rellinghaus, B.; Lafdi, K.; Schultz, L.; Buechner, B.; Ruemmeli, M. H. Catalyst Poisoning by Amorphous Carbon during Carbon Nanotube Growth: Fact or Fiction? *ACS Nano* **2011**, *5*, 8928−8934.

(13) Robertson, J. Amorphous Carbon. *Adv. Phys.* **1986**, *35*, 317−37.

(14) Muñoz, R.; Gómez-Aleixandre, C. Review of CVD Synthesis of Graphene. *Chem. Vap. Deposition* **2013**, *19*, 297−322.

(15) Teng, P.-Y.; Lu, C.-C.; Akiyama-Hasegawa, K.; Lin, Y.-C.; Yeh, C.-H.; Suenaga, K.; Chiu, P.-W. Remote Catalyzation for Direct Formation of Graphene Layers on Oxides. *Nano Lett.* **2012**, *12*, 1379−1384.

(16) Bhaviripudi, S.; Jia, X.; Dresselhaus, M. S.; Kong, J. Role of Kinetic Factors in Chemical Vapor Deposition Synthesis of Uniform Large Area Graphene Using Copper Catalyst. *Nano Lett.* **2010**, *10*, 4128−4133.

(17) Geiger, F.; Busse, C.; Loehrke, R. The Vapor Pressure of Indium, Silver, Gallium, Copper, Tin, and Gold between 0.1 and 3.0 bar. *Int. J. Thermophys.* **1987**, *8*, 425−436.

(18) Li, X.; Cai, W.; Colombo, L.; Ruoff, R. S. Evolution of Graphene Growth on Ni and Cu by Carbon Isotope Labeling. *Nano Lett.* **2009**, *9*, 4268−4272.

(19) Regan, W.; Alem, N.; Alemán, B.; Geng, B.; Girit, Ç; Maserati, L.; Wang, F.; Crommie, M.; Zettl, A. A Direct Transfer of Layer-Area Graphene. *Appl. Phys. Lett.* **2010**, *96*, 113102.

(20) Zhang, R.; Zhang, Y.; Zhang, Q.; Xie, H.; Wang, H.; Nie, J.; Wen, Q.; Wei, F. Optical Visualization of Individual Ultralong Carbon Nanotubes by Chemical Vapour Deposition of Titanium Dioxide Nanoparticles. *Nat. Commun.* **2013**, *4*, 1727.

(21) Shu, H.; Tao, X.-M.; Ding, F. What Are the Active Carbon Species during Graphene Chemical Vapor Deposition Growth? *Nanoscale* **2015**, *7*, 1627−1634.

(22) Li, X.; Zhu, Y.; Cai, W.; Borysiak, M.; Han, B.; Chen, D.; Piner, R. D.; Colombo, L.; Ruoff, R. S. Transfer of Large-Area Graphene Films for High-Performance Transparent Conductive Electrodes. *Nano Lett.* **2009**, *9*, 4359−4363.

(23) Wang, X.; Dolocan, A.; Chou, H.; Tao, L.; Dick, A.; Akinwande, D.; Willson, C. G. Direct Observation of Poly (Methyl Methacrylate) Removal from a Graphene Surface. *Chem. Mater.* **2017**, *29*, 2033−2039.

(24) Marsden, A. J.; Phillips, M.; Wilson, N. R. Friction Force Microscopy: a Simple Technique for Identifying Graphene on Rough Substrates and Mapping the Orientation of Graphene Grains on Copper. *Nanotechnology* **2013**, *24*, 255704.

DOI: 10.1021/jacs.9b02068
J. Am. Chem. Soc. 2019, 141, 7670−7674

(25) Nair, R. R.; Blake, P.; Grigorenko, A. N.; Novoselov, K. S.; Booth, T. J.; Stauber, T.; Peres, N. M.; Geim, A. K. Fine Structure Constant Defines Visual Transparency of Graphene. *Science* **2008**, *320*, 1308−1308.

DOI: 10.1021/jacs.9b02068
J. Am. Chem. Soc. 2019, 141, 7670−7674